

Some fundamentals of fluid mechanics

Dietrich Hummel

2.1 Properties of incompressible fluids

2.1.1 Density

The density of any material is defined as its mass per unit volume. In fluids this property depends on the pressure p and on the temperature T . The highest speeds achieved by land-vehicles during record attempts (Fig. 1.51) are in the order of the speed of sound, which is for air $a = 340 \text{ m/s} = 1225 \text{ km/h} = 765.6 \text{ mile/h}$. In the flow field of a body exposed to such a free stream the compressibility of the air, i.e. the variation of density due to changes of pressure and temperature, is very important. On the other hand, most vehicles including racing cars are operated at speeds V which are lower than one-third of the speed of sound. For this speed range the variations of pressure and temperature in the flow field vary little from those of the free stream values, and therefore the corresponding density changes can be neglected. Thus the fluid can be regarded as incompressible. In the case of air the density is a constant property, the numerical value of which is, according to US standard atmosphere sea-level conditions ($p = 1 \text{ atm}$, $T = 288 \text{ K}$)

$$\rho = 1.2250 \text{ kg/m}^3 (= \text{N s}^2/\text{m}^4)$$

2.1.2 Viscosity

Viscosity is caused by the molecular friction between the fluid particles; it relates momentum flux to velocity gradient, or applied stress to resulting

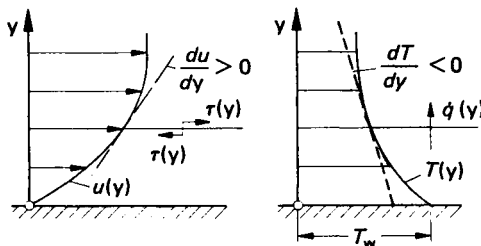


Figure 2.1 Distribution of velocity and temperature in the vicinity of a wall (schematic)

strain rate. According to Newton's law for the flow parallel to a wall (Fig. 2.1)

$$\tau = \mu \frac{du}{dy} \quad (2.1)$$

the shear stress τ is proportional to the velocity gradient du/dy . The constant factor μ is a property of the fluid and is called dynamic viscosity. In general its value depends on the temperature; see Schlichting.^{2,1} Often the quotient

$$\nu = \frac{\mu}{\rho} \quad (2.2)$$

is used, which is called kinematic viscosity and which depends on pressure and temperature. For incompressible fluids only, a temperature dependence exists for μ and ν . For air the US standard atmosphere sea-level values are

$$\mu = 1.7894 \times 10^{-5} \text{ N s/m}^2$$

$$\nu = 1.4607 \times 10^{-5} \text{ m}^2/\text{s}$$

The viscosity of a real fluid is the physical reason for the occurrence of a friction drag in the presence of a velocity gradient at a wall.

2.1.3 Thermal conductivity

This property of a fluid is connected with its ability to transport heat by conduction. Thermal conductivity relates heat flux to temperature gradient. According to Fourier's law

$$\dot{q} = -k \frac{dT}{dy} \quad (2.3)$$

the heat flux \dot{q} per unit area and time is proportional to the temperature gradient (Fig 2.1). The negative sign indicates that the heat flux is reckoned as positive in the direction of a negative temperature gradient. The constant k is a property of the fluid which is called thermal conductivity. In general its value depends on the temperature. For air, the US standard atmosphere value is

$$k = 0.0253 \text{ J/m s K} = \text{N/s K}$$

The thermal conductivity of a fluid is the physical reason for the heat transfer in the presence of a temperature gradient at a wall.

2.2 Flow phenomena related to vehicles

The various flow phenomena related to vehicles can be divided into two groups. These are (a) the external flow around the vehicle, including all details of its surface, and (b) the internal flow through different systems such as carburettor, engine, exhaust system and cooling system as well as the flow through the passenger cabin itself; see section 1.1.1.

2.2.1 External flow

The external flow around a vehicle is shown in Fig. 2.2. In still air, the undisturbed velocity V_∞ is the speed of the car. Provided no flow separation takes place, the viscous effects in the fluid are restricted to a thin layer of a few millimetres thickness, called the boundary layer. Beyond this layer the flow is inviscid and its pressure is imposed on the boundary layer. Within the boundary layer, the velocity decreases from the value of the inviscid external flow at the outer edge of the boundary layer to zero at the wall, where the fluid fulfils a no-slip condition. When the flow separates at the rear part of the vehicle (Fig. 2.2) the boundary layer is

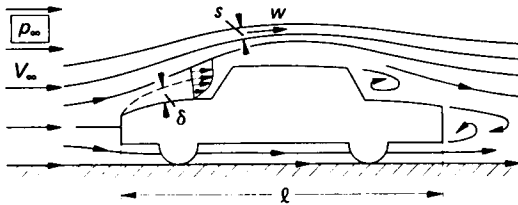


Figure 2.2 Flow around a vehicle (schematic)

‘dispersed’, and the flow is entirely governed by viscous effects. Such regions are quite significant compared with the characteristic length of the vehicle. At some distance from the vehicle, there exists no velocity difference between the free stream and the ground. Therefore, in vehicle-fixed coordinates, the ground plane is a stream surface with constant velocity V_∞ and at this surface no boundary layer is present. This fact is very important for the simulation of flows around vehicles in wind tunnels.

The boundary layer concept is only valid for large values of the order

$$Re_l = \frac{V_\infty l}{\nu} > 10^4 \quad (2.4)$$

This dimensionless parameter is called the Reynolds number. It is a function of the speed of the vehicle V_∞ , the kinematic viscosity ν of the fluid and a characteristic length of the vehicle, e.g. its total length l as in Fig. 2.2. The character of viscous flow around a body depends only on the body shape and the Reynolds number. For different Reynolds numbers entirely different flows may occur for the same body geometry. Thus the Reynolds number is the dimensionless parameter that characterizes a viscous flow.

Flows around geometrically similar bodies are called ‘mechanically similar’ if the Reynolds number according to Eqn 2.4 has the same value for different body lengths l , airspeeds V_∞ and fluid properties ν . Mechanical similarity is the basis for model tests. The results of tests on scale models in terms of dimensionless aerodynamic coefficients are the same as for the original vehicle if Reynolds numbers are the same; see section 11.4.2. Sometimes it is difficult to fulfil this similarity requirement. For models smaller than the original vehicle it is necessary to increase the free stream velocity V_∞ , but the value must remain in the low subsonic regime. This means that it is not possible to perform tests on very small

models in supersonic flow since the similarity law of compressible flow, which demands equal Mach numbers $Ma_\infty = V_\infty/a_\infty = \text{constant}$ for both cases, would then be violated.

Sometimes we need to investigate the flow around details such as a mirror, separate from the car. In such a case, correct results will be obtained if the tests are performed at the same Reynolds number as a characteristic dimension of this detail, for example the mirror's diameter, and on the local velocity in the vicinity of this detail at the vehicle, which is usually different from the free stream velocity; see Chapter 4.

2.2.2 Internal flow

Internal flow is that which is surrounded by walls. In the simple case of Fig. 2.3 all streamlines are parallel to the pipe axis. In general, internal flows cannot be divided into an inviscid flow far away from the walls and a

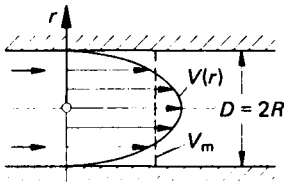


Figure 2.3 Velocity distribution of the flow through a pipe

viscous boundary-layer flow close to the walls. The effects of viscosity are found everywhere in the flow field. The development of an internal viscous flow is again characterized by the Reynolds number

$$Re_D = \frac{V_m D}{\nu} \quad (2.5)$$

based on a velocity typical for the problem, e.g. the mean velocity V_m as in Fig. 2.3, and the pipe diameter D as a typical length. For different values of Re_D , different types of flow may occur.

2.3 External flow problems

2.3.1 Basic equations for inviscid incompressible flow

The development of the inviscid flow at the outer edge of the boundary layer determines the pressure distribution on the body surface. Therefore the fundamentals of such a flow are discussed first.

To begin with, the law of mass conservation has to be formulated. The most simple form of this law is for incompressible flow ($\rho = \text{constant}$):

$$ws = \text{constant} \quad (2.6)$$

where s denotes the local cross-section of a small stream-tube as in Fig. 2.2 and w is the local velocity, which is assumed to be constant across s . Eqn 2.6 indicates narrow distances between the streamlines in regions of high velocity and vice versa, see Fig. 1.1.

Furthermore the flow obeys Newton's well-known law of momentum conservation: mass times acceleration is equal to the sum of the acting

forces. If this law is applied to an inviscid flow, it turns out that inertia forces and pressure forces are balanced. The integration of the momentum equation along a streamline for incompressible flow leads to

$$g = p + \frac{\rho}{2} w^2 = \text{constant} \quad (2.7)$$

Eqn 2.7 is Bernoulli's equation, which relates the pressure p and the velocity w along a streamline (p is static pressure, $\rho w^2/2$ is dynamic pressure, and g is total pressure).

In inviscid flow, the sum of static pressure and dynamic pressure is constant along a streamline. Eqn 2.7 indicates low pressure in regions of high local velocities and vice versa. If the flow comes to rest, $w = 0$, a so-called 'stagnation point', as on the nose of a vehicle (Fig. 2.2), the static pressure there will be equal to the total pressure, and this is the highest possible pressure in the flow field. For the external flow around a vehicle, as in Fig. 2.2, all streamlines start from the same free stream with static pressure p_∞ and free stream velocity V_∞ . Therefore the total pressure g is constant for all streamlines

$$g = p_\infty + \frac{\rho}{2} V_\infty^2 = \text{constant} \quad (2.8)$$

Such a flow field is called 'isoenergetic', and g is Bernoulli's constant of it.

2.3.2 Applications

The fundamental equations for inviscid flow may be applied to simple examples related to vehicle aerodynamics and experimental techniques.

The two-dimensional flow around a vehicle-shaped body is shown in Fig. 2.4. This flow is a considerable simplification of a three-dimensional flow around a vehicle, and may be regarded as a qualitative picture of the flow at the centre section of a car. The upper figure indicates the streamlines. Three stagnation points occur – in the nose region, in the corner between

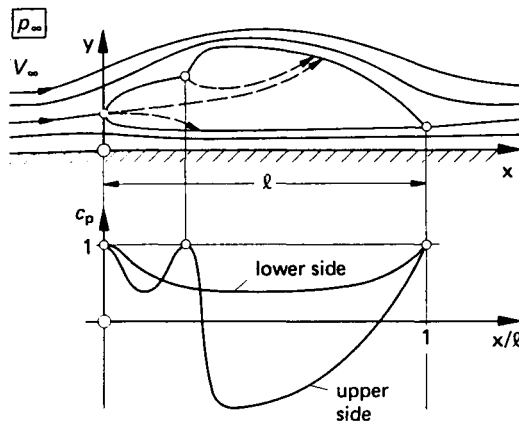


Figure 2.4 Flow field and pressure distribution for vehicle-shaped body in two-dimensional inviscid flow (schematic)

bonnet and windscreen, and at the trailing edge. The pressure distribution on the contour is drawn schematically as $c_p(x/l)$ in the lower figure, where

$$c_p = \frac{p - p_\infty}{\frac{\rho}{2} V_\infty^2} \quad (2.9)$$

is the dimensionless pressure coefficient. The application of Eqns 2.7 and 2.8

$$p + \frac{\rho}{2} w^2 = p_\infty + \frac{\rho}{2} V_\infty^2$$

leads to

$$c_p = \frac{p - p_\infty}{\frac{\rho}{2} V_\infty^2} = 1 - \left(\frac{w}{V_\infty} \right)^2 \quad (2.10)$$

In the stagnation points of the flow field, $w = 0$, Eqn 2.10 yields $c_p = 1$. At the lower surface of the vehicle, the pressure is higher than the free stream pressure, $c_p > 0$, but for very small ground distances even suction, $c_p < 0$, may be present. At the upper surface, high pressures, $c_p > 0$, are observed in the region of the bonnet and the windscreen, whereas high suction, $c_p < 0$, is found at the cabin roof. On the rear part of the vehicle's upper surface a steep pressure rise occurs, and it is in this region where considerable differences exist between the real flow of a viscous fluid and the inviscid flow shown here. The pressure distribution in Fig. 2.4 indicates that the pressure level on the upper side of the vehicle is much lower than on the lower side. This means that a net upwards lift force acts on the vehicle. If all x -components of the pressure distribution on the vehicle surface are integrated, the result for the drag will be $D = 0$. This is the well-known d'Alembert's paradox, which means that in incompressible, inviscid, two-dimensional flow no drag is present. In the real, viscous flow there exists a drag force, but it cannot be explained by considering an ideal, inviscid fluid.

From the pressure distribution shown in Fig. 2.4, suitable positions for the air intake and outlet for the cooling and ventilation system can be chosen. The intake may be placed in regions of high pressure, e.g. in the nose region or in front of the windscreen, whereas the outlet may be arranged in a region of suction. In this case the pressure difference can be

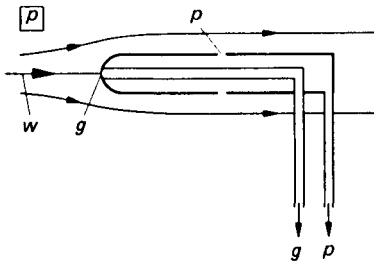


Figure 2.5 Pitôt-static probe for velocity measurements in fluids

used to assist the cooling and the ventilation systems, and fans can be kept small. Practical examples for this are discussed in Chapter 6.

As another example for the application of the basic equations of inviscid flows, the measurement of velocities may be considered. Figure 2.5 shows a Pitôt-static probe. At the tip of the probe a stagnation point occurs in the flow and from this point the total pressure g is taken through a small tube. A few diameters downstream of the tip of the probe, the static pressure p corresponding to the velocity w acts on the probe surface. This static pressure is taken through some holes around the circumference of the probe body. The application of Eqn 2.7 leads to

$$w = \sqrt{\left(\frac{2(g - p)}{\rho} \right)} \quad (2.11)$$

If the pressure difference $g - p$ is measured by manometer, the corresponding velocity can be calculated from Eqn 2.11. The Pitôt-static probe is widely used for velocity measurements in fluids, as well as for measurements of total pressure g (Pitôt probe) and static pressure p (static probe). In these cases the pressures g and p are measured separately against some reference pressure. To ensure accurate results the probe axis should be carefully aligned with the local flow direction; see section 12.1.2.

2.3.3 Effects of viscosity

Despite the thinness of the boundary layer at the wall, the viscous flow within it has a strong influence on the development of the whole flow field. The occurrence of drag in two-dimensional incompressible flow can only be explained by these viscous effects.

2.3.3.1 Laminar and turbulent boundary-layer development

The flow in a boundary layer along a thin flat plate is shown in Fig. 2.6. The corresponding external flow has parallel streamlines and constant velocity V_∞ and pressure p_∞ . The viscous flow within the boundary layer fulfils the ‘no-slip’ condition along the wall. In the front part of the plate the boundary layer flow is steady and (almost) parallel to the wall. This

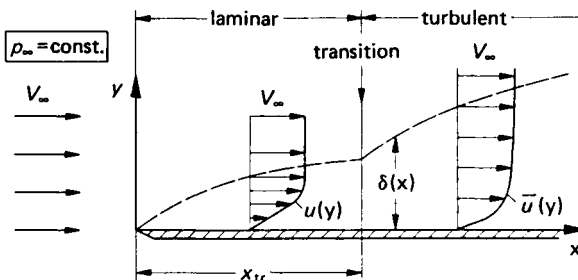


Figure 2.6 Boundary layer along a thin flat plate (dimensions in y -direction very much enlarged)

state of the flow is called laminar. The thickness of the boundary layer increases downstream according to

$$\delta \sim \sqrt{\left(\frac{\nu}{V_\infty}\right)} \cdot \sqrt{x} \quad (2.12)$$

With increasing distance x and kinematic viscosity ν and with decreasing free stream velocity V_∞ , the boundary layer thickness increases.

The laminar state of the boundary layer flow is stable against disturbances for certain conditions only. At a distance $x = x_{tr}$ from the leading edge of the plate a transition to the so-called turbulent state of the boundary layer takes place. The transition between the two states of the boundary layer flow is largely governed by the value of the Reynolds number. For the flat plate, transition occurs around

$$Re_{x_{tr}} = \frac{V_\infty x_{tr}}{\nu} = 5 \times 10^5 \quad (2.13)$$

but this value applies only for a negligible pressure gradient in the external flow. In cases with a pressure gradient, a pressure decrease in the flow direction leads to a stabilization of the laminar boundary layer, whereas an adverse pressure gradient causes an earlier transition to the turbulent state. Furthermore, disturbances of the laminar flow, e.g. by surface roughness, may lead to transition; see Schlichting.^{2,1} In general, for medium Reynolds numbers transition from laminar to turbulent occurs in the region of minimum pressure, and with increasing Reynolds number the transition point moves upstream.

In the region of the turbulent boundary layer the flow is basically unsteady. The time-averaged flow is still attached and (almost) parallel to the wall, but in addition to the mean velocity $\bar{u}(y)$, fluctuations u' , v' , w' are superimposed in all three coordinate-directions. The velocity component parallel to the wall in Fig. 2.6 is thus

$$u(y, t) = \bar{u}(y) + u'(y, t) \quad (2.14)$$

and $\bar{u}(y)$ is defined as

$$\bar{u}(y) = \frac{1}{\Delta t} \int_{t_0}^{t_0 + \Delta t} u(y, t) dt \quad (2.15)$$

where Δt is chosen so large that $\bar{u}(y)$ does not depend on Δt . Owing to the velocity fluctuations, intensive mixing takes place. Therefore, in addition to the shear stress caused by molecular friction according to Eqn 2.1, a shear stress due to turbulent mixing

$$\tau_{\text{turb}} = -\rho \overline{u'v'} \quad (2.16)$$

is present. In this expression u' and v' denote the velocity fluctuations in x - and y -directions and $\overline{u'v'}$ is the time-average derived from Eqn 2.15. Since u' and v' always have the opposite sign, the expression for τ_{turb} is always positive. The turbulent velocity fluctuations manifest themselves in an apparent increase in the viscosity of the fluid. Therefore the boundary

layer thickness along the flat plate in Fig. 2.6 increases more rapidly downstream of the transition point as

$$\delta \sim \sqrt[5]{\left(\frac{\nu}{V_\infty}\right)} x^{4/5} \quad (2.17)$$

Due to the mixing process in turbulent boundary layer flow, the velocity profiles show higher velocities close to the wall than in laminar flow.

2.3.3.2 Separation

Laminar and turbulent boundary layer flows depend strongly on the pressure distribution which is imposed by the external flow. For a pressure increase in flow direction the boundary layer flow is retarded, especially near the wall, and even reversed flow may occur. This behaviour is shown schematically in Fig. 2.7. It can be seen that, between forward and reverse

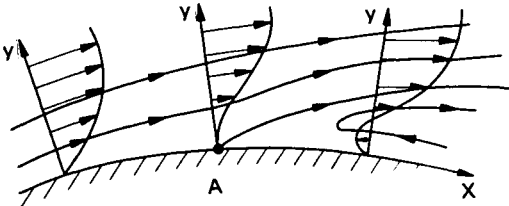


Figure 2.7 Separation of the boundary layer flow at a wall (schematic)

flow, a dividing streamline leaves the wall. This phenomenon is called separation. For the separation point A, the condition

$$\left(\frac{du}{dy}\right)_w = 0 \quad (2.18)$$

holds. Turbulent boundary layers can withstand much steeper pressure gradients without separation than can laminar boundary layers. This is because the turbulent mixing process leads to an intensive momentum transport from the outer flow towards the wall. For a pressure decrease in the flow direction there exists no tendency to flow separation.

2.3.3.3 Friction drag

If a velocity gradient du/dy is present in a viscous fluid at the wall, due to molecular friction a shear stress τ_w acts everywhere on the surface of a

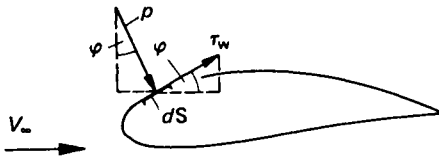


Figure 2.8 Determination of the drag of a body (example of two-dimensional flow)

body as indicated in Fig. 2.8. The integration of the corresponding force components in the free-stream direction according to

$$D_f = \oint \tau_w \cos \varphi \, dS \quad (2.19)$$

leads to the so-called friction drag D_f . In the absence of flow separation, this is the main contribution to the total drag of a body in two-dimensional viscous flow. Two examples may illustrate this.

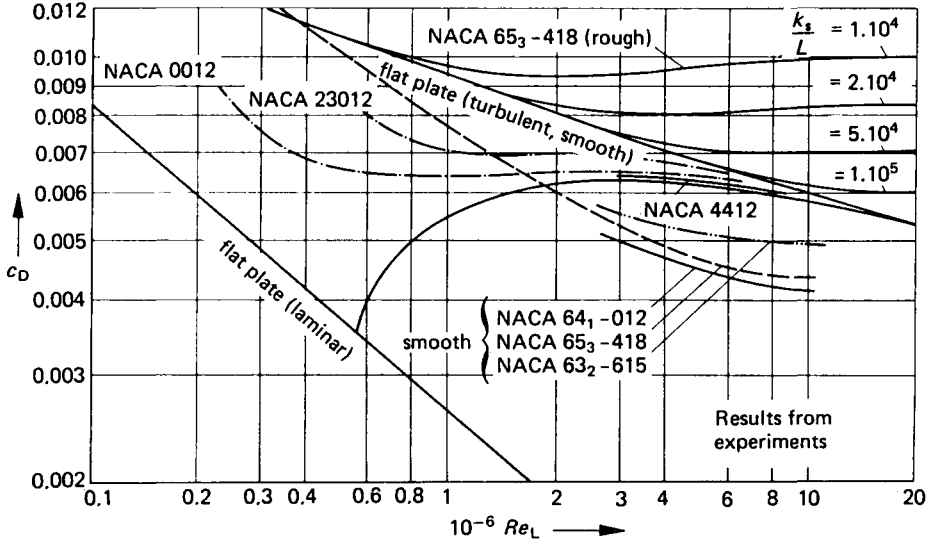


Figure 2.9 Drag coefficient for flat plates and aerofoils as a function of Reynolds number, from Schlichting^{2,1}

Figure 2.9 shows results for the flow along a thin flat plate of Fig. 2.6. In order to get results which do not depend on the actual dimensions (length l , width b) of the plate and on the free stream conditions (dynamic pressure $q_\infty = \rho V_\infty^2/2$), a dimensionless drag coefficient

$$c_D = \frac{D}{\frac{\rho}{2} V_\infty^2 b l} \quad (2.20)$$

is defined. In the case of a flat plate, only friction drag $D = D_f$ occurs on both sides of the plate. The planform area $b \times l$ is used as the reference area. In Fig. 2.9 the drag coefficient is plotted against Reynolds number $Re_l = V_\infty l/\nu$ based on the total length l of the plate or of the chord length l in the case of an aerofoil.

Results for flat plates are discussed first. For laminar boundary layers, the resistance law is

$$c_D = \frac{2.656}{\sqrt{(Re_l)}} \quad (\text{for } Re_l < 5 \times 10^5) \quad (2.21)$$

and for turbulent boundary layers over the whole length l of the plate and medium Reynolds numbers, the corresponding law is

$$c_D = \frac{0.148}{\sqrt[5]{(Re_l)}} \quad (\text{for } 5 \times 10^5 < Re_l < 10^7) \quad (2.22)$$

For even larger Reynolds numbers, an asymptotic law holds:

$$c_D = \frac{0.91}{(\log Re_l)^{2.58}} \quad (\text{for } Re_l > 10^7) \quad (2.23)$$

Assuming that the front part of the plate has a laminar boundary layer and the rear part a turbulent boundary layer, a transitional curve is derived, as shown in Fig. 2.9. For low Reynolds numbers this curve ends at the law for fully laminar flow, since no turbulent flow then occurs, and for high Reynolds numbers the transitional curve approaches asymptotically the law for fully turbulent flow, since the relative length of the laminar part decreases with increasing Reynolds number. In turbulent boundary layer flow, the friction drag is much higher than in the laminar case. This is because the turbulent mixing process leads to velocity profiles with a much steeper velocity gradient at the wall than in the laminar case. Furthermore, Fig. 2.9 indicates that in turbulent boundary layer flow the friction drag is increased by surface roughness. With increasing relative roughness k_s/l the drag coefficient increases and the dependence on the Reynolds number declines. A very rough plate behaves like the sum of a large number of blunt bodies. Details may be taken from appropriate textbooks (refs 2.1 to 2.7) and data works (refs 2.8 and 2.9).

The drag of bodies with finite thickness mainly consists of friction drag, which is small in all cases in which no flow separation occurs. This can be achieved by slender shapes on the rear part of the body which produce only a weak pressure rise in the flow direction. Shapes of this kind are aerofoils and 'streamlined' bodies. Some drag coefficients of aerofoils are drawn in Fig. 2.9. On the aerofoils NACA 0012, 4412 and 23012 the boundary layers are mainly turbulent and therefore the drag coefficients of these aerofoils are of the same order of magnitude as for the flat plate with fully turbulent boundary layer. Over large portions of the surface of the NACA-6 aerofoils the boundary layer is laminar and therefore the drag coefficients are considerably reduced.

Finally, Fig. 2.9 clearly indicates that the friction drag D_f in general depends strongly on the Reynolds number.

2.3.3.4 Pressure drag

Blunt bodies, such as a circular cylinder, a sphere or a flat plate normal to the flow, show quite different drag characteristics. On the rear part of such bodies in the inviscid external flow, extremely steep pressure gradients occur which lead to flow separation (Fig. 1.2). The pressure distribution is thereby considerably altered when compared with the theoretical case of inviscid flow. As an example, Fig. 2.10 shows the pressure distribution for a circular cylinder. In the front part the pressure distribution is similar to that in inviscid flow, whereas on the rear part the flow separation leads to considerable suction. The pressure distribution is therefore asymmetrical with respect to the y -axis. Integrating the force components in the free stream direction, resulting from the pressure distribution,

$$D_p = \oint p \sin \varphi \, dS \quad (2.24)$$

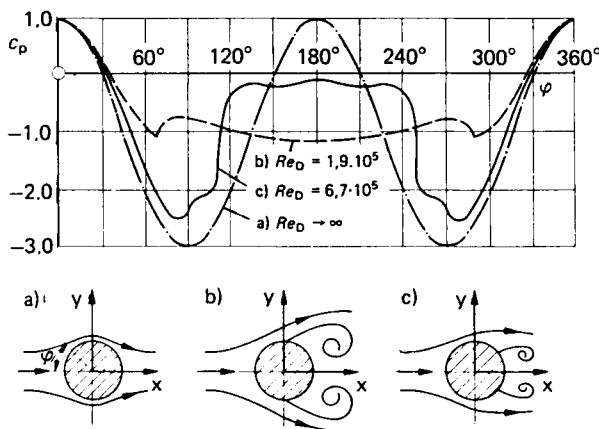


Figure 2.10 Pressure distribution and streamline pattern for a circular cylinder at different Reynolds numbers $Re_D = V_\infty D/\nu$: (a) inviscid flow; (b) sub-critical flow, boundary layer laminar; (c) supercritical flow, boundary layer turbulent.

gives the so-called ‘pressure drag’ D_p , see Fig. 2.8. Friction drag also results from the wall shear stresses, but for blunt bodies the pressure drag is predominant. In general, the drag of a body may be written as

$$D = D_f + D_p \quad (2.25)$$

For blunt bodies, the drag coefficient

$$c_{D,A} = \frac{D}{\frac{\rho}{2} V_\infty^2 A} \quad (2.26)$$

is based on the free stream dynamic pressure $\rho V_\infty^2/2$ and on the largest cross-section of the body, A . This is the projection of the body in a plane perpendicular to the free stream (frontal area).

Figure 2.11 shows this drag coefficient plotted against the Reynolds number $Re_D = V_\infty D/\nu$ for a circular cylinder and a flat plate. If very small

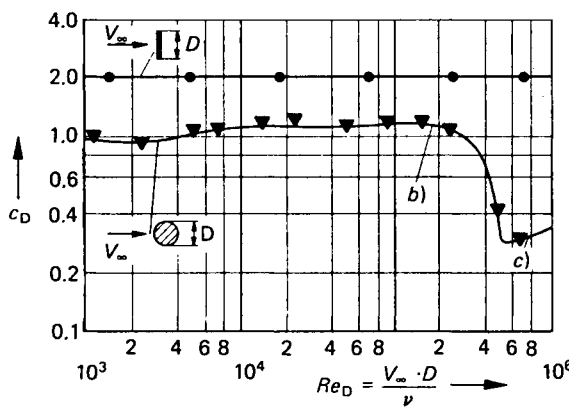


Figure 2.11 Drag coefficients of blunt bodies as a function of Reynolds number. Points (b) and (c) as in Fig. 2.10, two-dimensional flow

Reynolds numbers are excluded, for bodies with sharp edges flow separation will occur in the same way for all Reynolds numbers, and therefore the drag coefficients do not depend on the Reynolds number. However, for slightly rounded bodies, separation is not fixed and the position of the separation point depends on the state of the boundary layer. At low Reynolds numbers the boundary layer is laminar; see case (b) in Figs 2.10 and 2.11. The separation point is located close to the point of maximum thickness. The resulting 'wake' region behind the body is broad and the corresponding drag coefficient is high. At a critical Reynolds number of about $Re_{D,crit} = 5 \times 10^5$, a sudden transition to a turbulent boundary layer occurs in the front part of the body. The turbulent boundary layer remains attached longer; see case (c) in Figs 2.10 and 2.11. The corresponding wake region is narrow and the drag coefficient is much lower than for sub-critical Reynolds numbers.

Generally, a sudden change of the drag coefficient of a vehicle as a function of its Reynolds number should be avoided. For this purpose, flow separation is fixed at certain points, for instance at the upper edge of the sloping rear window. Up to this point the shape of the body should be designed so that the flow remains attached and that the pressure rise is as large as possible for various free stream conditions. The resulting wake should be as small as possible to obtain low drag. The drag coefficients achieved by present-day European cars (excluding sports cars and racing cars) range from 0.30 to 0.52; see Hucho.^{2,10} In general, the dependence of these drag coefficients on Reynolds number is very small and sudden changes do not occur. This demonstrates that the predominant part of the drag of these vehicles is pressure drag. For some unconventional 'streamlined' body shapes, drag coefficients have been measured in the region 0.15 to 0.27. For bodies of this type the portion of pressure drag is relatively small. These drag coefficients thus contain a large proportion of friction drag and therefore they depend noticeably on the Reynolds number; see Hucho.^{2,10}

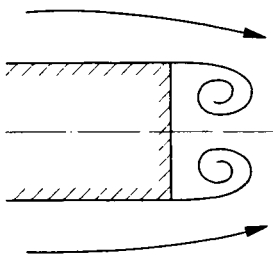


Figure 2.12 Flow separation on a bluff body (separation line perpendicular to the flow direction)

The flow separations that lead to a pressure drag can be divided into two different types. As shown in Fig. 2.12, the separation line may be located perpendicular to the flow direction. In this case, vortices are generated – the axes of which are also perpendicular to the outer flow. Thus the velocity components parallel to the vortex axes are very small. A symmetrical flow in the separated region as shown in Fig. 2.12 exists only for small Reynolds numbers, e.g. on a circular cylinder, for $Re_D < 60$; see Schlichting.^{2,1} For larger Reynolds numbers, periodic vortex shedding

occurs and the flow in the separated region is basically unsteady. The kinetic energy of the vortex field is rapidly dissipated by turbulent mixing and irreversibly converted into frictional heat. This leads to a considerable total pressure loss in the region behind the body and the corresponding deficit in kinetic energy is equal to the work which is necessary to overcome the pressure drag. Behind the body a wake is formed in which time-averaged, relatively uniform suction and very low flow velocities are present.

The other type of flow separation is characterized by a separation line inclined with respect to the oncoming flow, see Fig. 2.13. In this case, vortices are shed, the axes of which are roughly parallel to the separation lines. A considerable velocity component, parallel to the separation line

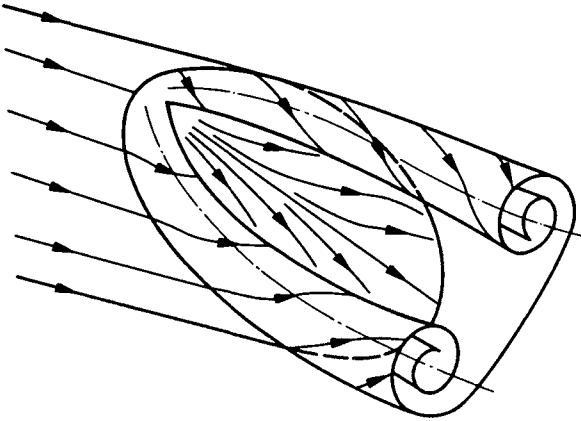


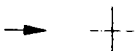

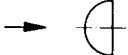
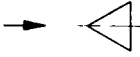
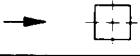
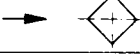
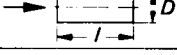
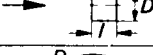
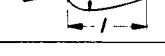

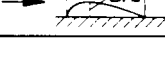
Figure 2.13 Flow separation on a body with oblique blunt base (separation line at an angle to the flow direction)

and therefore in the direction of the vortex axes, is present. Thus, a well-ordered, steady three-dimensional flow separation is found. On the rearward surface of the body this separated flow induces suction which leads to a pressure drag. On the inclined base of the body the flow is attached. In the vicinity of the vortices the pressure distribution is characterized by suction peaks. This kind of flow separation is well known in the aeronautical sciences from investigations on the flow field of delta wings; see the survey given by Hummel.^{2,11} Behind the body only relatively small total pressure losses are observed. The flow field of the concentrated vortices, however, contains a lot of kinetic energy which corresponds to the work necessary to overcome the pressure drag.

A relationship exists between both types of flow separation behind blunt bodies, which has already been investigated in the aeronautical sciences; see Thwaites^{2,12} and Hummel.^{2,11} As the angle of attack of a delta wing is increased a sudden change of the structure of the vortices is observed which is called 'vortex breakdown' or 'vortex bursting'. The phenomenon is not yet fully understood. It leads, however, to a destruction of the well-ordered three-dimensional vortex flow; this process starts in the vortex centre and spreads downstream over large portions of the vortex. The final state is a separated flow in the region of the vortex centre which is

embedded in a well-ordered three-dimensional flow. Systematic experimental investigations on vehicles with different inclinations of the rear surface have been carried out by Janssen and Hucho,^{2.13} Morel,^{2.14} and Ahmed.^{2.22,2.23} These investigations clearly indicated both types of flow separation. Transition from one type to the other leads to characteristic changes of the pressure drag which are also known from delta wings. This is discussed in detail in section 4.3.2.4.

Table 2.1 Drag coefficients for different bodies ($c_{D,c} = D/q_{\infty}S_c$, see Eqn 2.6, *subcritical flow), after Hoerner^{2.9}

Body	Flow situation	$c_{D,c}$
Circular plate		1.17
Sphere		0.47*
Half-sphere		0.42*
60°-cone		0.50
Cube		1.05*
Cube		0.80*
Circular cylinder $l/D > 2$		0.82
Circular cylinder $l/D > 1$		1.15
Streamlined body $l/D = 2,5$		0.04
Circular half-plate at a ground plane		1.19
Streamlined half-body at a ground plane		0.09

On the drag problem of a body, it might be mentioned finally that the shape of a body in front of the largest cross-section has only minor influence on the total drag. The main contributions to the drag force originate from the rear part of the body. It is not important to find a proper shape to divide the oncoming flow but it is very important to design a rear body surface which brings the divided streamlines smoothly together. Optimum shapes are 'streamlined' bodies having a very slender rear part. Table 2.1 lists some data on drag coefficients for different bodies.

2.3.3.5 Overall forces and moments

In addition to the drag discussed in detail so far, other forces and moments occur on a vehicle which are shown schematically in Fig. 2.14. In symmetrical flow ($\beta = 0$) the drag D is accompanied by a lift force L (see the pressure distribution of Fig. 2.4). Furthermore, a pitching moment M with respect to the lateral axis (y -axis) is present. The three components L , D and M completely determine the vector of the resulting airforce. For a known position of the centre of gravity, which is used as the pitching moment reference point, the additional forces acting at the front and rear axle resulting from the flow around the vehicle can easily be evaluated.

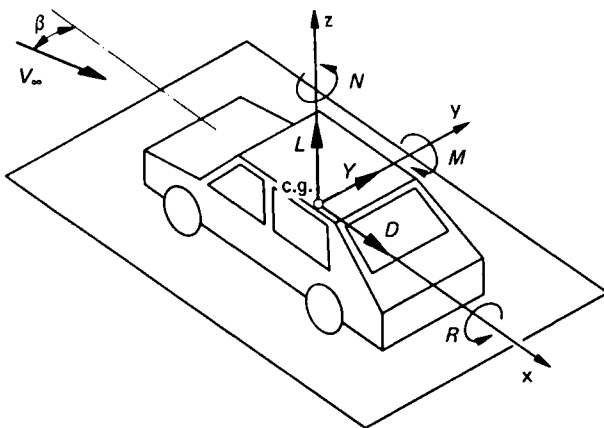


Figure 2.14 Forces and moments acting on a vehicle (c.g. = centre of gravity)

In cross-wind conditions ($\beta \neq 0$) an asymmetrical flow field around the vehicle is present. In this case, in addition to the forces and moments mentioned so far, a side force Y is observed. Furthermore, there occur a rolling moment R with respect to the longitudinal axis (x -axis) and a yawing moment N with respect to the vertical axis (z -axis). Thus six components L , D , M and Y , R , N determine the vector of the total force. For a known position of the reference point the additional forces acting at the four wheels of the vehicle can be evaluated.

The forces and moments acting on vehicles may be obtained from wind tunnel measurements on full-scale cars or on smaller models. Three- and six-component measurements are carried out in symmetrical and in asymmetrical flow respectively. In order to get results from model tests that are also valid for the full-scale vehicle, the Reynolds similarity law has to be fulfilled. This means that for both cases the Reynolds number,

$$Re_l = \frac{V_\infty l}{\nu}$$

from Eqn 2.4, has to be the same. The results will be independent of the actual dimensions of the tests, if dimensionless coefficients are formed by analogy with the drag coefficient as

$$c_L = \frac{L}{\frac{\rho}{2} V_\infty^2 A} \quad (\text{lift})$$

$$\begin{aligned}
c_D &= \frac{D}{\frac{\rho}{2} V_\infty^2 A} \quad (\text{drag}) \\
c_M &= \frac{M}{\frac{\rho}{2} V_\infty^2 A l} \quad (\text{pitching moment}) \\
c_Y &= \frac{Y}{\frac{\rho}{2} V_\infty^2 A} \quad (\text{side force}) \\
c_R &= \frac{R}{\frac{\rho}{2} V_\infty^2 A l} \quad (\text{rolling moment}) \\
c_N &= \frac{N}{\frac{\rho}{2} V_\infty^2 A l} \quad (\text{yawing moment})
\end{aligned} \tag{2.27}$$

All these coefficients are based on the free stream dynamic pressure $\rho V_\infty^2/2$ and on the largest cross-section, the frontal area A , of the body. In addition, a characteristic dimension such as the total length l of the vehicle is used for the three moments.

The dimensionless aerodynamic coefficients can only be dependent on other dimensionless parameters of the flow problem, e.g. on the Reynolds number Re_l or on the angle of yaw β . In this relation, a problem of stability occurs which may be explained for a vehicle in cross-wind, see section 5.2.3. In asymmetrical flow, a yawing moment acts on the body and the corresponding coefficient is c_N . This yawing moment has the tendency to rotate the vehicle about its vertical axis (z -axis). The vehicle is aerodynamically stable if the resulting yawing moment has the tendency to reduce the angle of yaw. With the notation of Fig. 2.14, this is valid for

$$\frac{dc_N}{d\beta} > 0 \quad (\text{stable}) \tag{2.28}$$

Conversely, the vehicle is aerodynamically unstable for

$$\frac{dc_N}{d\beta} < 0 \quad (\text{unstable}) \tag{2.29}$$

As will be shown in section 5.2.3, cars and box type vans generally are aerodynamically unstable. Only very long and thus unacceptable rear fins would lead to aerodynamic stability according to Eqn 2.28.

Similarly, as discussed for the drag coefficient, all other forces and moments may be influenced by proper shape of the vehicle. Without going into detail, some possibilities may be discussed. The shape of the car's underside has a large influence on the overall lift. With small ground clearances and a smooth shape of the lower surface, high velocities may be obtained between the vehicle and the ground. This leads to low pressures at the underside of the vehicle which keep the lift force small; see sections

7.3.1 and 7.4.1. Vortex type flow separations as in Fig. 2.13, related to inclined shapes of the base of a vehicle, may cause considerable contributions to the overall lift. Furthermore, the behaviour of vehicles in cross-wind conditions can be influenced quite strongly by proper shaping; see Hucho.^{2,15} For small angles of cross-wind, larger values of the yawing moment derivative $dc_N/d\beta$ may be allowed since the yawing moment N is still small and the main problem in this case is to reduce drag. For larger angles of yaw, the drag must be allowed to increase since the main problem is now to keep the yawing moment to a tolerable order of magnitude. How this can be achieved will be discussed in detail in section 5.2.3.

2.3.3.6 Thermal boundary layers

Like the velocity field of a viscous flow around a body, the temperature field has a boundary layer character. For instance, the region of increased temperature in the vicinity of a heated body is restricted to a thin layer close to the body. Such a thermal boundary layer is sketched in Fig. 2.15 for the simple flow along a flat plate. The corresponding velocity boundary layer is shown in Fig. 2.6. The wall temperature T_w of the heated plate may be kept constant. Within the thermal boundary layer of thickness δ_T , the temperature decreases to the value T_∞ in the outer flow.

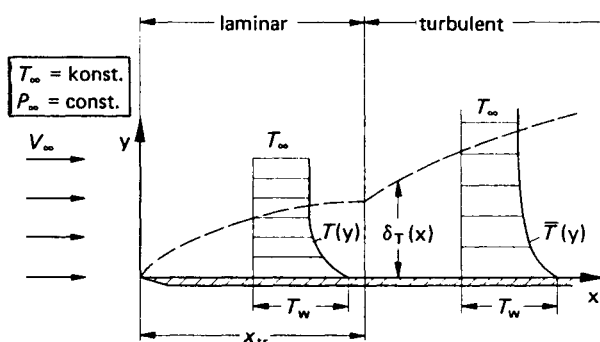


Figure 2.15 Thermal boundary layer along a thin flat plate (dimensions in y -direction very much enlarged)

For laminar flow according to Eqn 2.12 the thickness of the velocity boundary layer increases as $\delta \sim \sqrt{\nu}$; for incompressible flow ($\rho = \text{constant}$) this also means $\delta \sim \sqrt{\mu}$. By analogy, the corresponding result for the thickness of the thermal boundary layer is

$$\delta_T \sim \sqrt{k}$$

The ratio of the two boundary layer thicknesses is thus

$$\frac{\delta}{\delta_T} = \sqrt{\left(\frac{\mu c_p}{k}\right)} \quad (2.30)$$

In this equation c_p denotes the specific heat capacity for constant pressure of a gas; for liquids c_p may be replaced by the specific heat of the fluid. The expression $\mu c_p/k$ represents a dimensionless quantity

$$Pr = \frac{\mu c_p}{k} \quad (2.31)$$

which is called the Prandtl number. This parameter depends only on fluid properties. Its value is mainly governed by the ratio of dynamic viscosity and heat conductivity, which is actually the ratio of the fluid property for momentum transport to the fluid property for heat transport. The Prandtl number of air is $Pr \approx 0.7$. This means that in this case the two thicknesses of the velocity and the thermal boundary layer are of the same order of magnitude, and for approximations the Prandtl number can be set as $Pr = 1$. For other fluids, different values may apply: the Prandtl number for water is $Pr = 7$ ($\delta > \delta_T$) and for highly viscous oils $Pr = 10\,000$ ($\delta \gg \delta_T$).

In incompressible flows, no work is necessary for the compression of the fluid and the frictional heat produced by dissipation of kinetic energy is of minor importance for the temperature distribution in the boundary layer. The essentials are heat transport by thermal conduction according to Eqn 2.3 and heat transport by convection. This means that the temperature field depends on the velocity field, but the converse does not hold. A particularly simple situation is that of the flow along a flat plate as in Figs 2.6 and 2.15 with $p = p_\infty = \text{constant}$, and for the special case $Pr = 1$. For laminar flow the velocity profiles $u(y)$ and the temperature profiles $T(y)$ coincide in the dimensionless form

$$\frac{u(y)}{V_\infty} = \frac{T(y) - T_\infty}{T_w - T_\infty} \quad (2.32)$$

This function is shown in Fig. 2.16

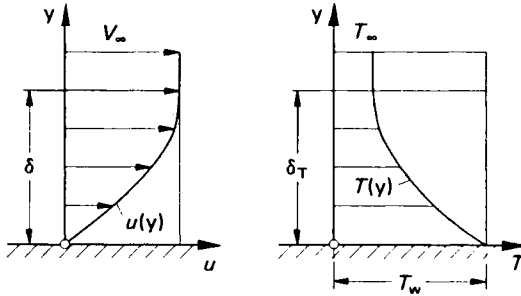


Figure 2.16 Velocity and temperature distribution in the laminar boundary layer along a flat plate without frictional heat and for $Pr = 1$ ($\delta = \delta_T$)

In Eqn 2.32 a relation between the velocity gradient at the wall $(du/dy)_w$ and the temperature gradient at the wall $(dT/dy)_w$ is demonstrated. This means that the shear stress at the wall according to Eqn 2.1 is related to the heat flux at the wall according to Eqn 2.3. After some calculation Eqn 2.32 yields

$$Nu(x) = \frac{1}{2} c_f'(x) Re_x \quad (2.33)$$

where $c_f'(x)$ is the dimensionless shear stress at the wall

$$c_f'(x) = \frac{\tau_w(x)}{\frac{\rho}{2} V_\infty^2} \quad (2.34)$$

Re_x is the Reynolds number $Re_x = V_\infty x / \nu$ based on the local distance x from the apex of the plate, and

$$Nu(x) = \frac{\dot{q}_w(x)x}{k(T_w - T_\infty)} \quad (2.35)$$

is the dimensionless heat flux at the wall, which is called the Nusselt number. The result according to Eqn 2.33 is the so-called Reynolds analogy between shear stress and heat flux at the wall. In section 9.5 it will be shown that experimental results on engine radiators can be arranged by application of the Nusselt number defined in Eqn 2.35.

In turbulent flows according to the mixing process an eddy heat flux

$$\dot{q}_{\text{turb}} = \rho c_p \overline{v'T'} \quad (2.36)$$

is observed by analogy to Eqn 2.16. The total shear stress and heat flux in turbulent flow is thus

$$\tau = \mu \frac{d\bar{u}}{dy} - \rho \overline{u'v'} = (\mu + A_\tau) \frac{d\bar{u}}{dy} \quad (2.37)$$

$$\dot{q} = -k \frac{d\bar{T}}{dy} + \rho c_p \overline{v'T'} = -(k + c_p A_q) \frac{d\bar{T}}{dy} \quad (2.38)$$

In these equations u' , v' , T' are the fluctuations derived in Eqn 2.14, and $\overline{u'v'}$ and $\overline{v'T'}$ denote time averages calculated for these quantities, as indicated in Eqn 2.15. The apparent increase of dynamic viscosity and heat conductivity is expressed in Eqns 2.37 and 2.38 by means of the exchange coefficients for momentum A_τ and heat A_q .

In addition to the molecular Prandtl number $Pr = \mu c_p / k$ it is convenient to introduce a corresponding, dimensionless, turbulent Prandtl number

$$Pr_t = \frac{A_\tau}{A_q} \quad (2.39)$$

which is important for the transport phenomena in turbulent flows. A good approximation for the turbulent Prandtl number is $Pr_t = 1$. This means that in turbulent flows the same mechanism for the eddy viscosity and the eddy conductivity is present. For the special case $Pr = 1$ and $Pr_t = 1$, which is approximately valid for air, the relation between velocity and temperature profiles according to Eqn 2.32 holds again; this means that the Reynolds analogy defined in Eqn 2.33 is also valid for the turbulent boundary layer along a flat plate as shown in Figs 2.6 and 2.15.

From Eqns 2.33, 2.34 and 2.35, the heat flux can be deduced as

$$\dot{q}_w = \frac{k(T_w - T_\infty)}{\delta} \cdot \frac{d(u/V_\infty)_w}{d(y/\delta)} \quad (2.40)$$

This equation demonstrates that the heat flux at the wall is proportional to the heat conductivity k of the fluid and is proportional to the imprinted

temperature difference $T_w - T_\infty$. In the front part, where the boundary layer thickness δ is small, high heat flux occurs. Downstream of the laminar/turbulent transition point the thickness of the turbulent boundary increases quite rapidly, but the corresponding increase of the velocity gradient of the turbulent velocity profiles at the wall is predominant. Therefore, in turbulent boundary layers, a higher heat flux at the wall is observed than in laminar boundary layers.

For many technical problems the situation is not as simple as in the case of the flow along a flat plate. Therefore Eqn 2.40 is often written as

$$\dot{q}_w = \alpha (T_w - T_\infty) \quad (2.41)$$

and the special problem is now found in the new heat transfer coefficient α which may be taken from the literature for different flow conditions.^{2,16}

2.3.4 Special problems

2.3.4.1 Aerodynamic noise

The flow around a vehicle causes aerodynamic noise; see section 6.5. In almost all cases the physical reason is periodic flow separation from certain elements of the surface – gutters, mirrors and the radio antenna, for instance. Such a periodic flow separation is sketched for a circular cylinder in Fig. 2.17. It is present in the Reynolds number range $60 \leq Re_D \leq 5000$. For smaller Reynolds numbers a non-periodic, symmetrical wake (as in Fig. 2.10) occurs, whereas for larger Reynolds numbers a turbulent mixing process without the existence of discrete vortices can be observed.

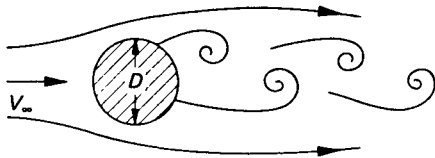


Figure 2.17 Periodic vortex shedding from a circular cylinder (schematic)

In the region of periodic flow separations, vortices are shed from both sides of the body in alternating sequence. These vortices move downstream in the wake and they can be observed over a long distance. In a coordinate system moving downstream with the vortices, a regular pattern of these vortices is found, which is called a von Karman's vortex street. Due to periodic vortex shedding, the whole flow field is basically unsteady. At a certain point of the flow field, all flow quantities change with the frequency n of the vortex separation from the body. The dimensionless frequency is an important parameter

$$St = \frac{nD}{V_\infty} \quad (2.42)$$

which is called the Strouhal number. This parameter is a unique function of the Reynolds number which is shown in Fig. 2.18 for a circular cylinder. For $Re > 10^3$ the Strouhal number is practically independent of the Reynolds number and its value is $St = 0.21$. A simple calculation for

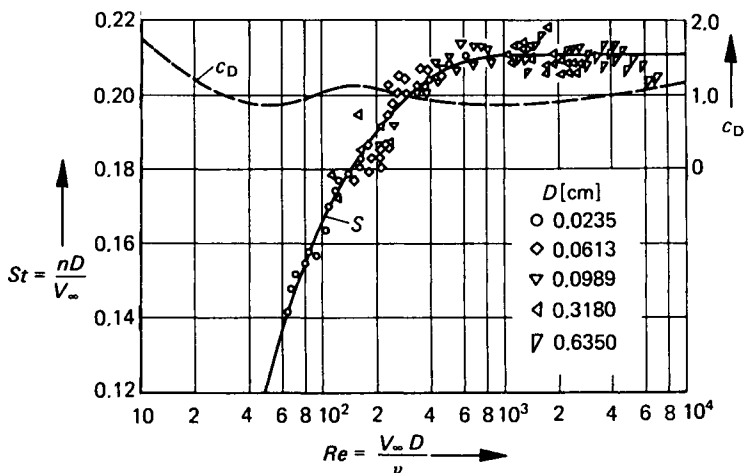


Figure 2.18 Strouhal number as a function of Reynolds number for the flow around a circular cylinder, from Schlichting^{2.1}

$$\begin{aligned}
 D &= 4 \text{ mm} \\
 V_{\infty} &= 5 \text{ m/s} \\
 \nu &= 1.461 \times 10^{-5} \text{ m}^2/\text{s} \\
 Re &= V_{\infty} D / \nu = 1369 \\
 n &= St V_{\infty} / D = 262 \text{ 1/s}
 \end{aligned}$$

shows that the resulting frequency lies in the audible range, so that pressure fluctuations within the unsteady flow field manifest themselves as noise.

Preventive measures against such noise are (a) to avoid inducing the flow separations and (b) to disturb the periodic wake flow by proper means. A survey of the present knowledge on airframe noise has recently been given by Heller and Dobrzynski.^{2.17}

2.3.4.2 Aeroelastic effects

These problems arise when aerodynamic forces acting on an elastic body cause elastic deformation of the body which influences the inducing aerodynamic forces.

The static aeroelastic problems will be considered first. The aerodynamic loading causes a deformation and the new geometry leads to modified aerodynamic forces. The final deformation is reached for equilibrium between aerodynamic and elastic forces. An example of this kind of problem is the deformation of a radio antenna due to wind loads. The modifications of the aerodynamic forces result from the fact that the deflected flow is no longer perpendicular to the axis of the antenna. If velocity is increased, the static aeroelastic forces will also increase and at a certain speed the antenna will fracture.

Much more difficult to understand are the dynamic aeroelastic problems. Consider a body in a periodic motion of a certain frequency. In the presence of a flow the corresponding aerodynamic forces are also periodic with the same frequency. During the motion of the body the

aerodynamic forces may act in the direction of motion or against it. If the oscillating system, time-averaged over the whole period of the motion, does not absorb energy from the flow, no danger of self-excited oscillations exists. As an example of this kind (Fig. 2.19) the combined beating and twisting oscillations of a flat plate are considered. Without a phase difference between the two motions, i.e. if maximum stroke and maximum twist occur simultaneously, the aerodynamic force partly acts in the direction of motion and partly against it. Therefore, when time-averaged, no work is done by the aerodynamic forces. But there exist other situations for which the aerodynamic forces perform work at the oscillating system.

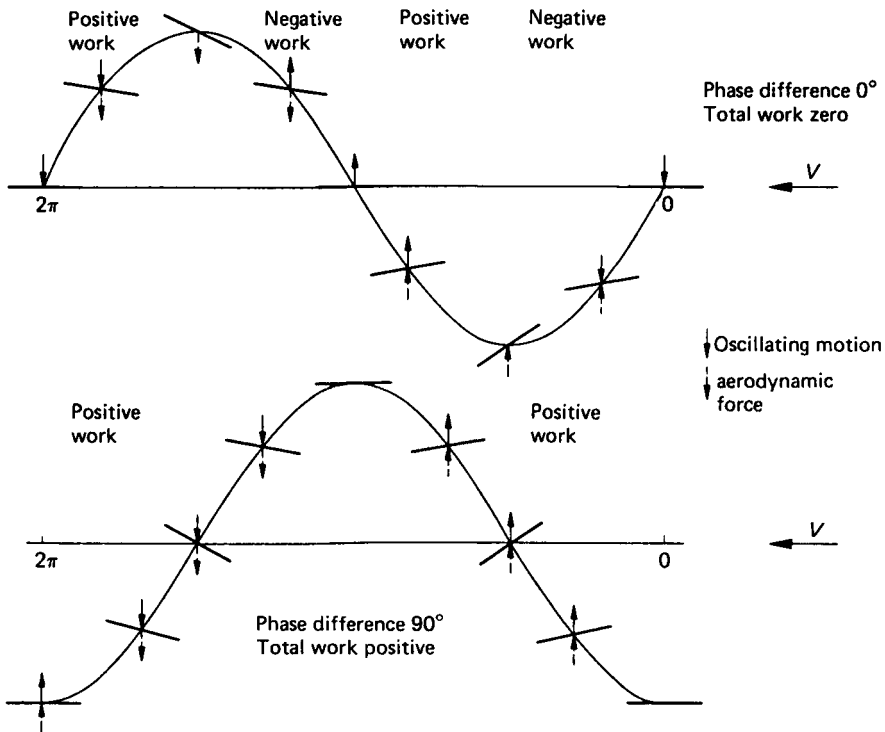


Figure 2.19 Energy balance for a flat plate with combined beating and torsional oscillations (schematic), after Försching^{2,18}

In the bottom example of Fig. 2.19 the phase difference between beating and twisting motion is 90° and the maximum twist is present for zero stroke. In this case the aerodynamic force always acts in the direction of motion. Therefore a self-excited oscillation occurs, called flutter. In such a situation the inner damping of the elastic system is no longer sufficient to maintain stability and an abrupt instability of the whole system is observed.

In the example of Fig. 2.19 the aerodynamic forces result from the unsteady attached flow around the flat plate. There also exist flutter effects for which the stimulating aerodynamic forces are due to periodic flow separations on the rear part of the body. Details cannot be discussed here, but may be taken from the survey on these problems given by Försching.^{2,18}

2.3.4.3 Transport of solids

The flow around a vehicle may contain different inhomogeneities such as rain drops, mud particles and insects. The behaviour of these inhomogeneities in the flow field of the vehicle are very important for the practical use of the vehicle; see sections 6.4 and 8.7.

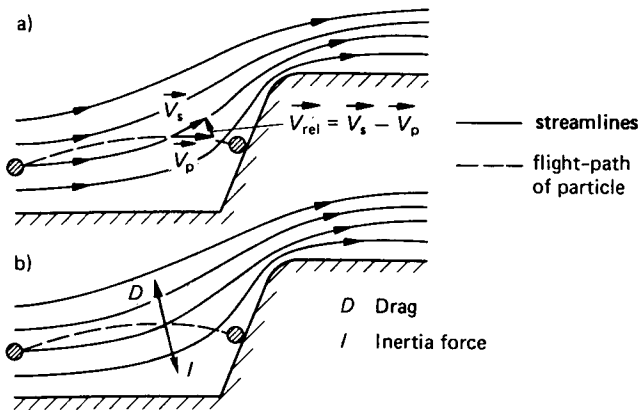


Figure 2.20 Particle motion in a flow field: (a) velocity vectors; (b) acting forces

The motion of particles in a flow field, the density of which is different from that of the fluid, is sketched in Fig. 2.20. The flight paths of the particles and the streamlines are different. For an arbitrarily located point of the flow field the local flow velocity \vec{V}_s is tangential to the streamline and the local particle velocity \vec{V}_p is tangential to the flight path. Thus the flow around the particle is governed by the relative velocity

$$\vec{V}_{\text{rel}} = \vec{V}_s - \vec{V}_p \quad (2.43)$$

and the drag force D acts on the particle in the direction of this relative velocity. For asymmetrical particle shapes a lift force may also be present, but this is not taken into account for the present considerations. The flight path and the velocity of the particle on it have to adjust in such a way that the inertia force I resulting from this motion compensates for the drag of the particle, as indicated in Fig. 2.20. This inertia force contains the gravitational acceleration as well as all other accelerations resulting from the changes in magnitude and direction of the velocity vector. In the vicinity of a body the gravitational acceleration can often be neglected, i.e. the weight of the particles need not be taken into account.

The problem of the determination of particle flight paths in a flow field has not yet been treated comprehensively in the literature. Some references may be taken from Brun,^{2,19} who investigated the motion of small droplets in the flow field of a wing in connection with the problem of icing. But this problem is a special case since droplets in fog and clouds have a negligibly small vertical velocity in the atmosphere. Therefore in the free stream there exists no relative velocity between the flow and the droplets. In more general cases, such as for instance for falling rain drops

or whirled-up mud already in the free stream far away from the vehicle, considerable relative velocities are present.

For the determination of the flight paths of the particles, and for the estimation of the amount of mud on the surface of a vehicle, the three-dimensional flow field must first be known. Up to the present, this problem has not been solved sufficiently and in the necessary detail by aerodynamic theory. Therefore experimental investigations are necessary, which may be performed either on the road or in a wind tunnel for real conditions. If experiments are carried out on models smaller than the original vehicle, the question of the corresponding similarity rules arises. For a mechanically similar flow field the Reynolds number

$$Re_l = \frac{V_\infty l}{\nu} = \text{constant} \quad (2.44)$$

must be constant. If the weight of the particles can be neglected, the same flight paths are obtained (see Brun^{2.19}) if the parameter

$$\Psi = \frac{\rho}{\rho_p} \frac{l}{d_p} = \text{constant} \quad (2.45)$$

is constant. In this equation, ρ/ρ_p is the ratio of the density of the fluid ρ to the density of the particles ρ_p and l/d_p denotes the ratio of the characteristic length of the vehicle l to the characteristic dimension d_p of the particles. If both equations are fulfilled simultaneously, this leads – for the case of the same fluid ($\nu_1 = \nu_2$) for model (2) and original (1) and for a length scale l_1/l_2 – to

$$V_{\infty 2} = \frac{l_1}{l_2} V_{\infty 1} \quad (2.46)$$

If particles of the same kind are used ($\rho_{p1} = \rho_{p2}$), the size of the particles has to be chosen so that

$$d_{p2} = \frac{l_2}{l_1} d_{p1} \quad (2.47)$$

This means that for experiments on smaller models, smaller particles have to be used – which is difficult to handle.

For the interpretation of experimental results the basic ideas considered so far are important. Accumulation of mud on the surface of a vehicle occurs due to the fact that the mud particles are not able to follow the streamlines – especially in regions of high streamline curvature. The flight paths of the mud particles show relatively low curvature up to the impact on the vehicle surface. This effect is present for instance in the highly curved flows between the bonnet and the windscreen in the front part as well as in the vortex flow over the rear part of a vehicle.

2.4 Internal flow problems

2.4.1 Basic equations for incompressible flow

As already mentioned in section 2.2.2, fully developed internal flows cannot be split up into an inviscid outer flow and a viscous boundary layer

flow close to the wall. In general, the viscous effects extend over the whole cross-section. Therefore, in the equations of motion, the viscous forces have to be taken into account from the beginning.

To start with, the law of mass conservation can be written, for a flow as shown in Fig. 2.3, as

$$\rho \int_{(S)} V dS = \text{constant} \quad (2.48)$$

This means that the mass flow through the cross-section $S(x)$ is constant along x . If a mean velocity is introduced by

$$V_m = \frac{1}{S} \int_{(S)} V dS \quad (2.49)$$

the equation of continuity may be written in the form

$$\rho V_m S = \text{constant} \quad (2.50)$$

by analogy to Eqn 2.6. For constant density ρ the mean velocity is high in narrow cross-sections and vice versa.

For internal flows Newton's law is also valid but, in addition to the pressure forces, viscous forces have to be considered. Figure 2.21 shows as

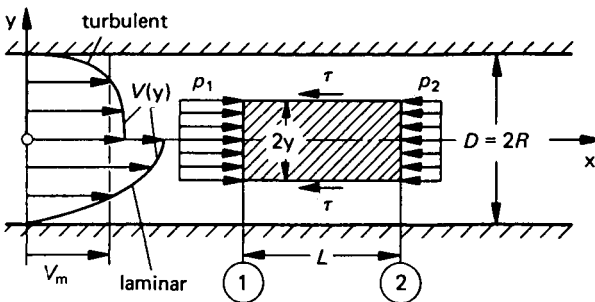


Figure 2.21 Laminar and turbulent pipe flow

a simple example the fully developed flow through a cylindrical pipe. In this case the velocity distribution $V(y)$ is the same for all cross-sections; $x = \text{constant}$. No acceleration is present in the flow and therefore no inertia forces occur. The pressure is constant over the cross-section and, due to the friction forces, a pressure difference $p_1 - p_2 > 0$ between the two sections 1 and 2 must exist to move the fluid against the friction drag through the pipe. This means that the friction effects cause a pressure decrease in flow direction which is called the pressure loss due to friction Δp . If this pressure loss is taken into account, Bernoulli's equation, Eqn 2.7, can be written in extended form as

$$p_1 + \frac{\rho}{2} V_{m1}^2 = p_2 + \frac{\rho}{2} V_{m2}^2 + \Delta p \quad (2.51)$$

In this equation the internal flow is regarded as a one-dimensional problem. The pressure p and the mean velocity V_m are constant over the

cross-section S and all quantities depend only on the coordinate x in the flow direction. Eqns 2.51 and 2.7 are only valid for flows in which no or only negligibly small variations of the geodetic height occur. If such variations are taken into account, terms resulting from hydrostatics have to be added on each side of Eqn 2.51, which yields

$$p_1 + \frac{\rho}{2} V_{m1}^2 + \rho g h_1 = p_2 + \frac{\rho}{2} V_{m2}^2 + \rho g h_2 + \Delta p \quad (2.52)$$

In this formula h_1 and h_2 are the geodetic heights of the streamtube at the stations 1 and 2. In viscous flow, the sum of static pressure ($p + \rho g h$) and dynamic pressure $\rho V_m^2/2$ is not constant. The total pressure decreases downstream by the pressure loss Δp caused by viscosity.

In general the pressure loss Δp is related to the dynamic pressure $\rho V_{m1}^2/2$ (sometimes also to $\rho V_{m2}^2/2$) which leads to a dimensionless loss coefficient

$$\zeta = \frac{\Delta p}{\frac{\rho}{2} V_{m1}^2} \quad (2.53)$$

This loss coefficient is different for various internal flow problems and its value is in general also a function of the Reynolds number. The loss coefficient is a criterion for the quality of cooling ducts and radiators; see sections 9.4.1 and 9.5.1. Some important elements of cooling systems will be discussed subsequently.

2.4.2 Applications

2.4.2.1 Laminar and turbulent pipe flow

At a certain distance downstream of the entrance of a pipe, the velocity distribution over the cross-section ceases to change. This state is called the fully developed pipe flow, which is sketched in Fig. 2.21. The equation of continuity, Eqn 2.50, is thus fulfilled and for a horizontal pipe ($h_1 = h_2$, $V_{m1} = V_{m2}$) Eqn 2.52 yields

$$p_1 - p_2 = \Delta p \quad (2.54)$$

In this case no inertia forces are present. From the equilibrium of pressure forces and viscous forces shown in Fig. 2.21

$$\tau(y) = \frac{p_1 - p_2}{2l} y \quad (2.55)$$

can be deduced. Thus the distribution of the shear stress across the pipe cross-section is linear. This result is valid for laminar as well as for turbulent pipe flow.

For Reynolds numbers $Re_D = V_m D/\nu < 2300$ laminar flow is found in a pipe. With the notation of Fig. 2.21 Newton's law, Eqn 2.21, can be written as

$$\tau = -\mu \frac{dV}{dy} \quad (2.56)$$

Combining Eqns 2.55 and 2.56, integration can be carried out and the well-known parabolic velocity distribution

$$V(y) = \frac{p_1 - p_2}{4\mu l} (R^2 - y^2) \quad (2.57)$$

results, for which the mean velocity according to Eqn 2.49 can be calculated as

$$V_m = \frac{p_1 - p_2}{32\mu l} D^2 \quad (2.58)$$

For the loss coefficient ζ_p in a pipe Eqn 2.53 yields

$$\zeta_p = \frac{\Delta p}{\frac{\rho}{2} V_m^2} = 64 \frac{\mu}{\rho V_m D} \cdot \frac{l}{D} \quad (2.59)$$

The loss coefficient is proportional to the length/diameter ratio of the pipe. In order to get an expression which is independent of l and D the so-called frictional resistance

$$\lambda = \frac{D}{l} \zeta_p \quad (2.60)$$

is introduced and, with this notation, Eqn 2.59 reads

$$\lambda = \frac{64}{Re_D} \quad (2.61)$$

This function is shown in Fig. 2.22. It is in excellent agreement with experimental data.

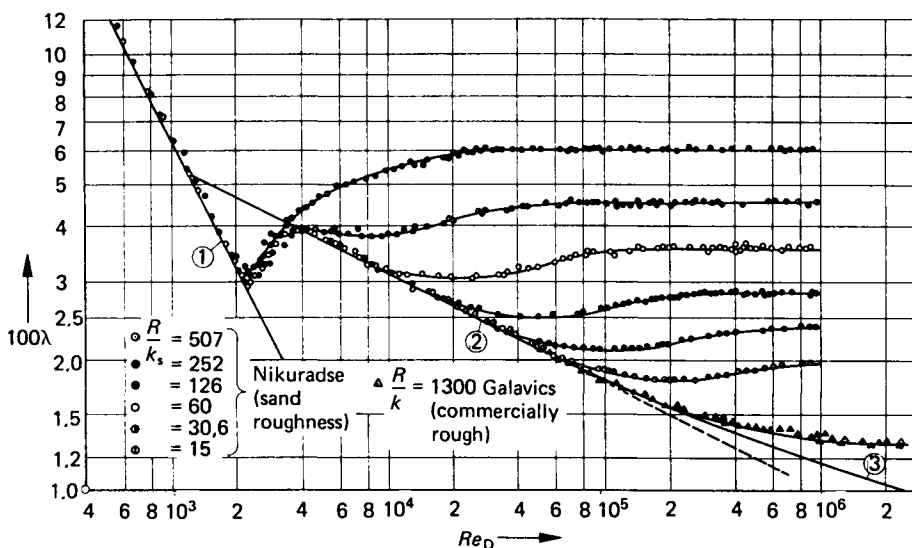


Figure 2.22 Frictional resistance in pipes, from Schlichting²⁻¹: (1) laminar, Eqn 2.61; (2) turbulent, Eqn 2.92; (3) turbulent, Eqn 2.63

For $Re_D > 2300$ the pipe flow is turbulent. As we already know from the flow along a flat plate, the velocity profiles in turbulent flow show higher velocities close to the wall than those in laminar flow. The calculation of these velocity distributions is rather complicated since for turbulent flow Eqn 2.56 has to be replaced by another expression, Eqn 2.37 for the shear stress. The frictional resistance of pipes for turbulent flow is, according to Schlichting,^{2,1}

$$\lambda = \frac{0.3164}{\sqrt[4]{Re_D}} \quad \text{for } 2.3 \times 10^3 < Re_D < 10^5 \quad (2.62)$$

and

$$\frac{1}{\sqrt{\lambda}} = 2 \cdot \log (Re_D \sqrt{\lambda}) - 0.8 \quad \text{for } Re_D > 10^5 \quad (2.63)$$

These functions are also drawn in Fig. 2.22.

The flow through a pipe is an internal flow problem without any flow separation. The resistance is due to pure friction drag. By analogy to the flow along a flat plate, the frictional resistance depends strongly on the Reynolds number. In Fig. 2.22 the frictional resistance is also shown for rough pipes. As in the case of a flat plate (see Fig. 2.9), surface roughness further increases the drag and the frictional resistance becomes independent of the Reynolds number. This is because flow separations occur on the roughness elements. Therefore a rough surface behaves like the sum of a large number of bluff bodies, see Fig. 2.11. Further details may be taken from the literature, refs. 2.1 to 2.9.

The flow through pipes having non-circular cross-sections can be related to an equivalent pipe flow with circular cross-sections. For given dimensions of the non-circular pipe (cross-sectional area S , circumferential length U) the diameter of the equivalent circular pipe is given by

$$D_{eq} = \frac{4S}{U} \quad (2.64)$$

2.4.2.2 Curved pipes

Flow separations may also occur in pipes. As an example, the flow in a curved pipe is shown in Fig. 2.23. The deflection of the flow by the walls is induced by a pressure gradient perpendicular to the streamlines. In a curved pipe, the pressure at the outer radius is higher and at the inner radius is lower than the pressure in the flow upstream and downstream.

Table 2.2 Loss coefficients ζ_c for curved pipes (from ref. 2.8. See Fig. 2.23 for notation)

δ	0°	15°	22.5°	45°	60°	90°
ζ_c	$r/D = 1$	0	0.03	0.045	0.14	0.19
	$r/D = 2$	0	0.03	0.045	0.09	0.12
	$r/D = 4$	0	0.03	0.045	0.08	0.10
	$r/D = 6$	0	0.03	0.045	0.075	0.09

Therefore a danger of flow separation, caused by pressure increase in the flow direction, is present at the outer radius close to the entrance and at the inner radius near the exit of the curved pipe, as indicated in Fig. 2.23.

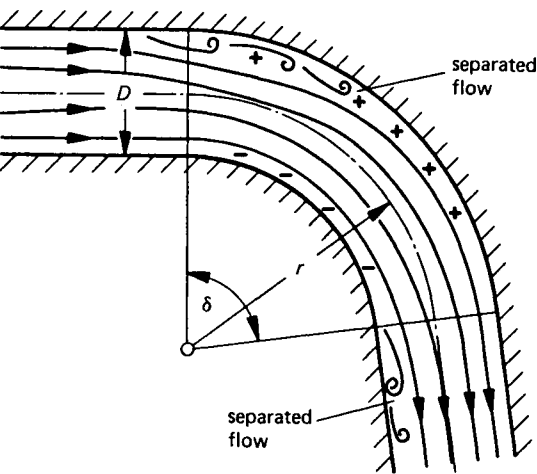


Figure 2.23 Flow in a curved pipe

These effects increase with decreasing curvature radius r and with increasing angle δ . Due to the flow separations, loss coefficients ζ_C according to Eqn 2.53 occur that are almost independent of the Reynolds number. This means that a quadratic resistance law, $\Delta p \sim V_m^2$, exists – which is well-known for bluff bodies as in Fig. 2.11. Values for curved pipes taken from ref 2.8 are shown in Table 2.2. They indicate that for $\delta > 45^\circ$ low loss coefficients ζ_C can only be achieved by a large curvature radius r compared to the pipe diameter D .

2.4.2.3 Inlets

The flow through an inlet (Fig. 2.24) may also cause total pressure losses Δp . Especially for sharp-edged inlets, flow separations occur and the corresponding values for the loss coefficients ζ_I according to Eqn 2.53 are

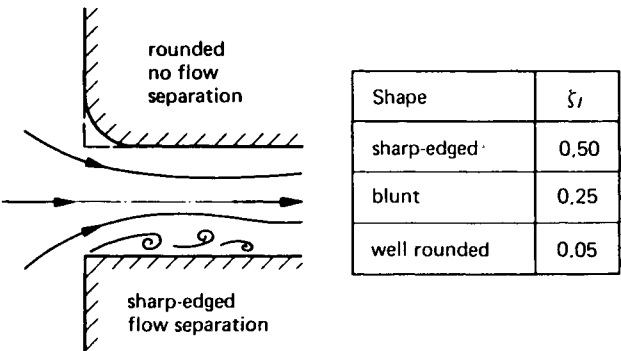


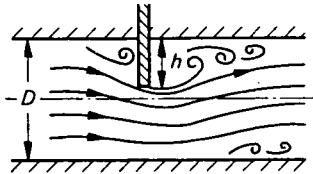
Figure 2.24 Flow field and loss coefficients^{2,8} for inlets

high. The values in the small table in Fig. 2.24 indicate that, to achieve small loss coefficients, inlets have to be well rounded rather than sharp-edged.

2.4.2.4 Local contractions

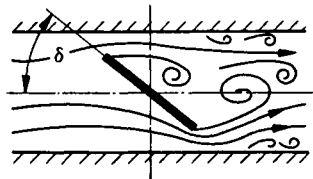
Local reductions of the cross-sectional area – for instance in sleeve valves, flap valves etc. – are used to control the flow rate in pipes, e.g. in the control of heating and cooling systems, see section 10.4.4. Two examples

a) Sleeve valve



Position h/D	ζ_s
0	0
0.25	0.26
0.50	2.1
0.75	17.0
0.87	98.0

b) Flap valve



Position $\delta [^\circ]$	ζ_F
0	0
10	0.52
20	1.54
40	10.8
60	110
70	751

Figure 2.25 Flow field and loss coefficients^{2,8} in valves: (a) sleeve valve; (b) flap valve

are shown in Fig. 2.25. In the local contractions, high velocities (see the continuity equation, Eqn 2.50) and low pressures (see Eqn 2.51) are present. On the rear part of the element, which produces the contraction, the flow separates. Downstream of the smallest cross-section the pressure increases at the walls and the flow may separate there too. The corresponding loss coefficients are extremely high – especially for nearly closed positions of the valves.

Local contractions of the cross-sectional area can also be used to measure the flow rate through a pipe. A well-known example of this kind is an orifice meter in which the flow field is much as sketched in Fig. 2.25 for a sleeve valve. The loss coefficient ζ_O of an orifice-meter depends strongly on the area ratio and on the shape of the edges of the orifice, but does not depend on the Reynolds number. For a known value of the loss coefficient ζ_O , Eqn 2.53 can be used to determine the mean velocity V_m and thus the flow rate from the measured pressure loss Δp . Details may be found in the literature, especially refs. 2.3, 2.6 and 2.8.

2.4.2.5 Cross-section enlargements

In cross-section enlargements, as shown in Fig. 2.26, the mean velocity decreases in flow direction according to the continuity equation

$$V_{m2} = \frac{S_1}{S_2} V_{m1} \quad (2.65)$$

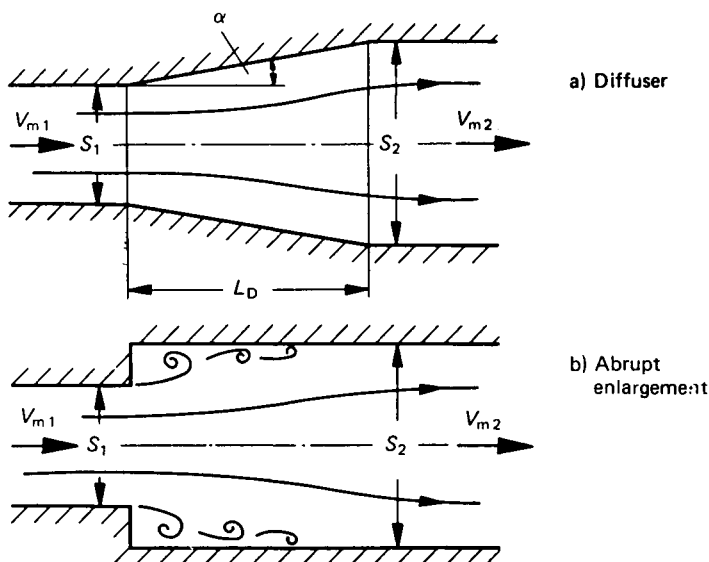


Figure 2.26 Flow through cross-section enlargements: (a) diffuser; (b) abrupt enlargement

This means that a pressure rise in flow direction is present and therefore flow separations may occur. In non-viscous flow the largest possible pressure increase would be, according to Eqn 2.51, for $\Delta p = 0$

$$p'_2 - p_1 = \frac{\rho}{2} V_{m1}^2 \left[1 - \left(\frac{S_1}{S_2} \right)^2 \right] \quad (2.66)$$

Due to the viscous effects in real flow, only a smaller pressure increase $p_2 - p_1$ is achieved and the corresponding pressure loss is

$$\Delta p = p'_2 - p_2 \quad (2.67)$$

For gradual cross-section enlargements in diffusers having small angles $2\alpha < 8^\circ$, the flow remains attached. In this case the pressure losses Δp are proportional to the theoretical value for the pressure increase $p'_2 - p_1$, which can be written as

$$\frac{\Delta p}{\frac{\rho}{2} V_{m1}^2} = \zeta_D = \varepsilon \frac{p'_2 - p_1}{\frac{\rho}{2} V_{m1}^2} \quad (2.68)$$

with $\varepsilon = 0.05$ to 0.3 . Using Eqn 2.66 leads to

$$\zeta_D = \varepsilon \left[1 - \left(\frac{S_1}{S_2} \right)^2 \right] \quad (2.69)$$

The loss coefficient ζ_D of a diffuser depends on the area ratio S_1/S_2 while the factor ε is a function of the relative length of the diffuser l_D/D_1 , of the diffuser shape and of the velocity distribution at the diffuser inlet. In the case of attached flow, a particular theory is available, see Truckenbrodt,^{2,7} and Schlichting and Gersten.^{2,20} Comprehensive experimental data on flows in diffusers have been published by Sprenger.^{2,21}

For larger diffuser angles 2α , the flow separates and the loss coefficients are much greater. The limiting case of an abrupt cross-section enlargement is also shown in Fig. 2.26. For this case, a particular theory is also available; see Truckenbrodt.^{2,7} In the absence of viscosity the theoretical pressure rise is given by

$$p_{2th} - p_1 = \rho V_{m2} (V_{m1} - V_{m2}) \quad (2.70)$$

Compared to the largest possible value according to Eqn 2.66, a pressure loss Δp_{th} can be calculated for inviscid flow from Eqn 2.67 as

$$\Delta p_{th} = \frac{\rho}{2} (V_{m1} - V_{m2})^2 \quad (2.71)$$

and the corresponding theoretical loss coefficient for an abrupt cross-section enlargement $\zeta_{A th}$ is

$$\zeta_{A th} = \frac{\Delta p_{th}}{\frac{\rho}{2} V_m^2} = \left(1 - \frac{S_1}{S_2}\right)^2 \quad (2.72)$$

In real viscous flow, still higher loss coefficients

$$\zeta_A = \beta \zeta_{A th} = \beta \left(1 - \frac{S_1}{S_2}\right)^2 \quad (2.73)$$

occur and the factor $\beta = 1.1$ to 1.2 .

A comparison of the results according to Eqns 2.69 and 2.73 leads to the conclusion that small cross-section enlargements may be designed as abrupt ones, since in this case the loss coefficients are not larger than those for a diffuser. For high area ratios a diffuser has to be designed, but in vehicles the length l_D necessary for a good diffuser design unfortunately is often not available and in this case higher loss coefficients have to be taken into account; see section 9.4.1.

2.5 Relationships between external and internal flow on vehicles

For a vehicle, external and internal flow are closely related; see Fig. 2.4. The system for cooling the engine, for instance, may use the pressure difference in the external flow between the stagnation region in the front part of the vehicle and the low pressure region on its underside; see Chapter 9. Similarly, for the ventilation of the passenger compartment, the pressure difference between the stagnation region in front of the windscreen and the ventilation exits at the rear end of the passenger cabin may be used; see Chapters 6 and 10.

The pressure differences utilized by these systems are proportional to the square of the speed of the vehicle V . They are not present for the vehicle at rest and they are maximum for maximum speed. The mass flow of the internal flow adjusts in such a way that the sum of all pressure losses Δp of the involved elements is equal to the pressure difference which exists between inlet and exit. Therefore the mass flow rate depends strongly on the speed of the vehicle. The link between the external and internal flows is

the fact that, at the inlet and at the outlet of the internal flow system, the pressure is the same for the external and the internal flow.

However, the mass flow through the internal flow system may cause changes in the external flow. At the inlet of the internal flow system, suction of the external flow takes place and, at the outlet of the internal flow system, blowing into the external flow is present. The amount of the interference depends on the mass flow rate of the internal flow and the corresponding effects need not be adverse. For instance, blowing over well-designed exhaust slits may cause favourable effects in the boundary layer of the external flow.

The dependence of the available pressure difference on the speed of the vehicle is rather disadvantageous since for low speeds only very small mass flow rates through the internal flow systems occur. Therefore, in the cooling system of the engine (see Chapter 9) as well as for the ventilation of the passenger cabin (see Chapter 10), additional fans are used, which ensure a certain mass flow rate ρQ even for zero velocity of the vehicle. The pressure difference necessary to overcome all pressure losses Δp has to be provided by the fan and the corresponding power is

$$P = Q \Delta p \quad (2.74)$$

where Q is the volume rate in m^3/s . In order to keep this additional power as small as possible the internal flow system has to be designed for low loss coefficients in all its parts. The use of powerful fans may lead to increased interference between the internal and the external flow and to noise.

2.6 Notation

A	cross-sectional (frontal) area
A_v, A_q	exchange coefficients; Eqns 2.37 and 2.38
D	diameter ($D = 2R$)
D	drag; Fig. 2.14
D_f	friction drag; Eqn 2.19
D_p	pressure drag; Eqn 2.24
I	inertia force; Fig. 2.20
L	lift; Fig. 2.14
M	pitching moment, reference point and sign; Fig. 2.14
N	yawing moment, reference point and sign; Fig. 2.14
Nu	local Nusselt number; Eqn 2.35
P	power; Eqn 2.74
Pr	Prandtl number; Eqn 2.31
Q	volume rate
R	radius ($R = D/2$)
R	rolling moment, reference point and sign; Fig. 2.14
Re	Reynolds number
Re_D	Reynolds number, based on a diameter ($= V_\infty D/\nu$ external flow problem, $V_m D/\nu$ internal flow problem)
Re_l	Reynolds number, based on a length in flow direction ($= V_\infty l/\nu$)
Re_x	Reynolds number, based on the distance x from apex ($= V_\infty x/\nu$)
S	cross-sectional area of ducts
St	Strouhal number; Eqn 2.42

T	temperature
T'	temperature fluctuation; Eqn 2.14
U	circumferential length of a non-circular cross-section
V	flow velocity
V_m	mean velocity; Fig. 2.21 and Eqn 2.49
Y	side force; Fig. 2.14
a	speed of sound
b	width of plate; Eqn 2.20
c_D	drag coefficient
c'_f	dimensionless shear stress at the wall; Eqn 2.34
c_L	lift coefficient
c_M	pitching moment coefficient
c_N	yawing moment coefficient
c_P	pressure coefficient; Eqn 2.9
c_p	specific heat capacity at constant pressure; Eqn 2.30
c_R	rolling moment coefficient
c_Y	side force coefficient
d	particle size in Eqn 2.45
g	total pressure
h	geodetic height in Eqn 2.52
k	thermal conductivity; Eqn 2.3
k_s	height of roughness elements; Fig. 2.9
l	characteristic length; Fig. 2.2
n	frequency
p	static pressure
q	dynamic pressure
\dot{q}	heat transfer per unit area and time; Eqn 2.3
r	radial coordinate; Fig. 2.3
s	local area of a stream-tube; Fig. 2.2
t	time
u, v	velocity components in x -, y -direction
u', v', w'	velocity fluctuations; Eqn 2.14
w	local flow velocity; Fig. 2.2
x, y, z	rectangular coordinates
α	heat transfer coefficient, Eqn 2.41
β	angle of yaw, Fig. 2.14
δ	boundary layer thickness, Fig. 2.6
ζ	loss coefficient, Eqn 2.53
λ	coefficient of frictional resistance in a pipe, Eqn 2.60
μ	dynamic viscosity, Eqn 2.1
ν	kinematic viscosity, Eqn 2.2
ρ	density
τ	shear stress, Eqn 2.1
φ	angle, Figs 2.8 and 2.10
Ψ	parameter, Eqn 2.45

Subscripts

∞	free steam conditions
crit	critical quantity

m	mean value
p	quantity related to a solid particle
rel	relative quantity
s	quantity acting parallel to the streamlines
t	quantity acting parallel to the flight path of a solid particle
th	theoretical quantity
tr	quantity related to laminar/turbulent transition
turb	quantity related to the turbulent state of the flow
w	quantity at the wall ($y = 0$)
A	abrupt cross-section enlargement
C	curved pipe
D	diffuser
F	flap-valve
I	inlet
O	orifice-meter
P	pipe
S	sleeve valve
T	quantity related to the thermal boundary layer
\rightarrow	vector
$\bar{}$	time-averaged value, Eqn 2.15